LA-UR-19-25669
Approved for public release; distribution is unlimited.

Title: Models for HEU objects in the NDSE IV and III series

Author(s): Lestone, John Paul
Andrews, Madison Theresa

Intended for: Share results to colleague

Issued: 2019-06-19

Models for HEU objects in the NDSE IV and III series

J. P. Lestone and M. T. Andrews

XCP-3, Los Alamos National Laboratory

May 10th, 2019

Introduction

A Neutron-Diagnosed Subcritical Experiment (NDSE) proof-of-principle setup exists at area-11 in Nevada [1]. An exquisite set of gamma-ray flux die-away data has been obtained at this facility for a number of highly-enriched uranium (HEU) objects, including objects referred to as IV, IV′, IV″ (the object IV series), IIIa, and IIIb (the object III series) [2]. These objects are constructed via a set of hemi-spherical concentric HEU shells (known as the Rocky Flats shells), surrounded by a sphere of aluminum (Al), encased in an outer sphere of high-density polyethylene (HDP) [3]. Bulk properties of object IV are listed in Table I.

Table I. Bulk properties of Object IV.

	HEU	Al	HDP
Outer radius (cm)	7.33	7.66	9.68
Mass (kg)	30	0.5	1.8

The "as built" detailed MCNP-calculated k_{eff} values obtained by Goorley, for the object IV and III series, are listed in Table II. These model calculations contain detailed information about the inner and outer radii and masses of each hemi-shell used to make each of the objects. Objects IV′, and IV″ were obtained by replacing inner HEU shells with Al. The low k_{eff} of object IIIa was obtained by substituting a single HEU shell, with an inner radius of ~5 cm, with an Al shell. For object IIIb the substitution was a little further out but only in one hemi-shell. Except for the inner most shell (ball), all HEU shells have a thickness close to 0.333 cm.

Table II. MCNP calculated k_{eff} values [3] for the object IV and III series.

Object	IV	IV′	IV″	IIIa	IIIb
k_{eff} (MCNP)	0.9313	0.9144	0.9179	0.902	0.912

Previously [4] the k_{eff} of objects IV′, IV″, IIIa, and IIIb, were determined from measured gamma-ray die-away data via an analysis using a simple modification of the density of the HEU in our simple three layered model (HEU, Al, and HDP) of object IV including the outer safety can [4]. This was done to see the quality of the inference and investigate any limitations associated with not using detailed information about the known perturbations used to make these objects. In this work, we built models (priors) of objects IV′, IV″, IIIa, and IIIb that make use of our knowledge about the nature of the perturbations (see Fig. 1). With these models, instead of adjusting the

density of the HEU in our object IV model to match the data from objects IV′, IV″, IIIa, and IIIb, as done previously [4], we will be able to (in future studies) adjust r_{AL}, and r_i to infer the k_{eff} of the corresponding objects (see Fig. 1).

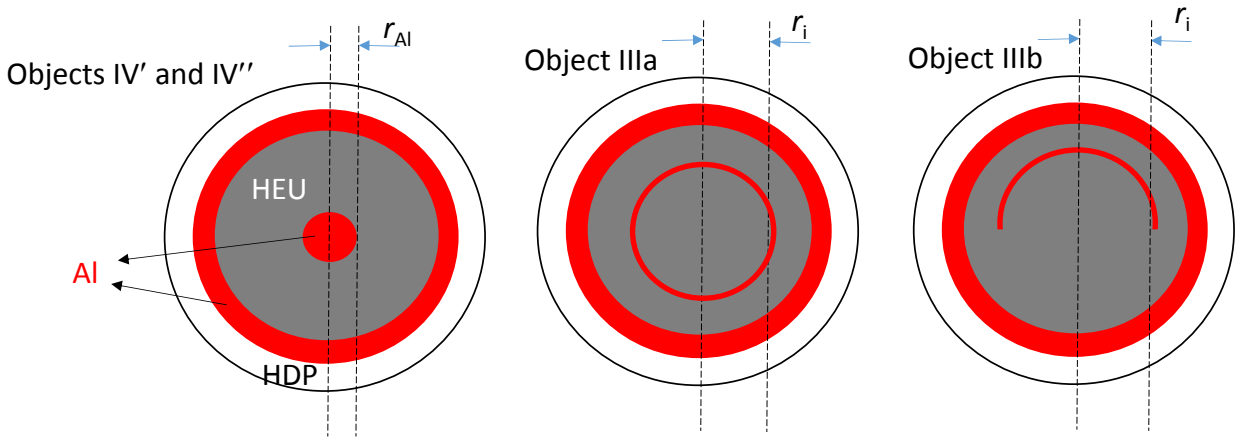

Fig. 1. Schematic representation of our priors for objects IV′, IV″, IIIa, and IIIb. The outer radii of the central Al ball in objects IV′, IV″ is r_{Al}. The inner radius of the shell and hemispherical shell in objects IIIa and IIIb is r_i. The thicknesses of these Al shells are 0.333 cm.

Object IV model

Object IV is the same as objects IV′ and IV″ displayed in Fig. I, but with the central Al ball radius set to r_{Al}=0. The orange circles in Fig. 2 show MCNP calculations of the k_{eff} of object IV as a function of the assumed density of the HEU. This covers the range of k_{eff} values for the seven objects previously studied at area-11 and is the model used previously to infer k_{eff} values for these objects. The dashed curve shows a quadratic fit to the orange circles. The red "x"s display test calculations that were not used to obtain the fit. Table III lists the relationship between HEU density and k_{eff} for object IV obtained via the quadratic fit. The ρdr changes between neighboring elements in Table III are ~0.3%. Therefore, these calculations demonstrate that a k_{eff} uncertainty of 0.002 corresponds to an effective ρdr uncertainty of ~0.3% (for object IV).

Table III. The relationship between HEU density and k_{eff} for object IV obtained using the quadratic fit displayed in Fig. 2.

k_{eff}	0.892	0.894	0.896	0.898	0.900	0.902	0.904	0.906	0.908	0.910
ρ (g/cc)	16.9521	17.0008	17.0496	17.0986	17.1478	17.1970	17.2465	17.2960	17.3457	17.3956
k_{eff}	0.912	0.914	0.916	0.918	0.920	0.922	0.924	0.926	0.928	0.930
ρ (g/cc)	17.4456	17.4957	17.5461	17.5965	17.6471	17.6979	17.7488	17.7999	17.8512	17.9026
k_{eff}	0.932	0.934	0.936	0.938	0.940	0.942	0.944	0.946	0.948	0.950
ρ (g/cc)	17.9542	18.0100	18.0601	18.1105	18.1613	18.2124	18.2639	18.3157	18.3679	18.4205
k_{eff}	0.952	0.954	0.956	0.958	0.960					
ρ (g/cc)	18.4734	18.5267	18.5805	18.6346	18.6892					

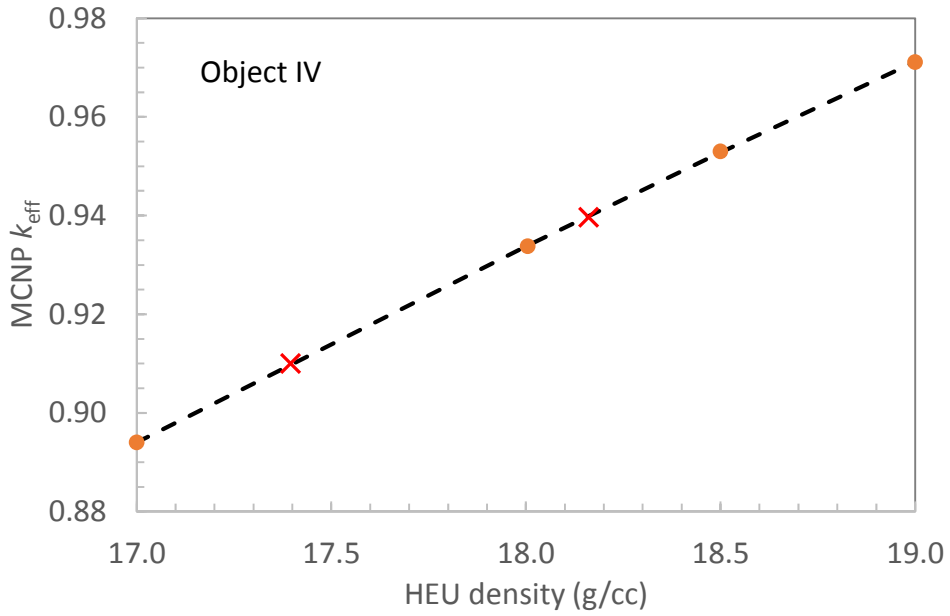

Fig. 2. MCNP calculated k_{eff} vs the object IV HEU density (symbols). The dashed curve shows a quadratic fit to the orange circles. The orange circles were used to obtain the quadratic fit. The red crosses show MCNP test calculations not used in obtaining the fit.

Model for objects IV′ and IV″

This new model is based on the prior shown in Fig. 1 and has not yet been used to infer k_{eff} values of objects IV′ and IV″ from the corresponding experimental gamma-ray flux die-away curves measured at area-11. Instead, the above discussed object IV model with HEU density modifications (see Fig. 2) has been used [4]. The MCNP calculated k_{eff} values for the new model are given as a function of Al ball mass and radius in figures 3 and 4 (with all material densities held fixed). Notice the k_{eff} vs Al mass relationship appears less complex than the k_{eff} vs radius relationship. For this reason a quadratic fit was performed in the k_{eff} vs mass space, and then mapped onto the k_{eff} vs radius space to obtain the values listed in Table IV.

Table IV. The relationship between k_{eff} for objects IV′ and IV″ and the radius of the central Al ball.

k_{eff}	0.880	0.882	0.884	0.886	0.888	0.890	0.892	0.894	0.896	0.898
r_{Al} (cm)	2.8338	2.7868	2.7397	2.6923	2.6445	2.5963	2.5475	2.4979	2.4475	2.3961
k_{eff}	0.900	0.902	0.904	0.906	0.908	0.910	0.912	0.914	0.916	0.918
r_{Al} (cm)	2.3435	2.2895	2.2340	2.1766	2.1172	2.0553	1.9906	1.9226	1.8505	1.7735
k_{eff}	0.920	0.922	0.924	0.926	0.928	0.930	0.932			
r_{Al} (cm)	1.6905	1.5998	1.4990	1.3841	1.2481	1.0761	0.8226			

Although we show calculations with a central Al ball radius less than 2 cm, we know the minimum possible radius is ~2 cm. For Al ball radii > 2 cm the neighboring elements in table IV

have Al radii that differ by ~50μm. These calculations demonstrate that a k_{eff} uncertainty of 0.002 corresponds to an effective uncertainty in the inference of an Al-HEU boundary deep inside a near-critical object of ~50 μm with a boundary radius > 2 cm.

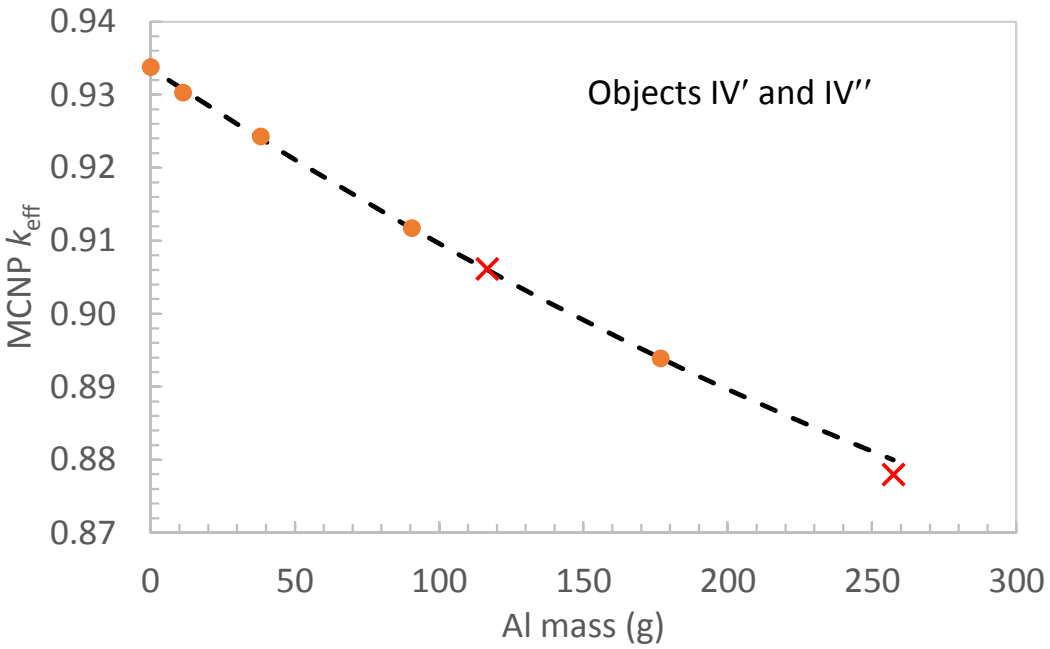

Fig. 3. MCNP calculated k_{eff} vs the mass of a central Al ball (symbols). The dashed curve shows a quadratic fit to the orange circles.

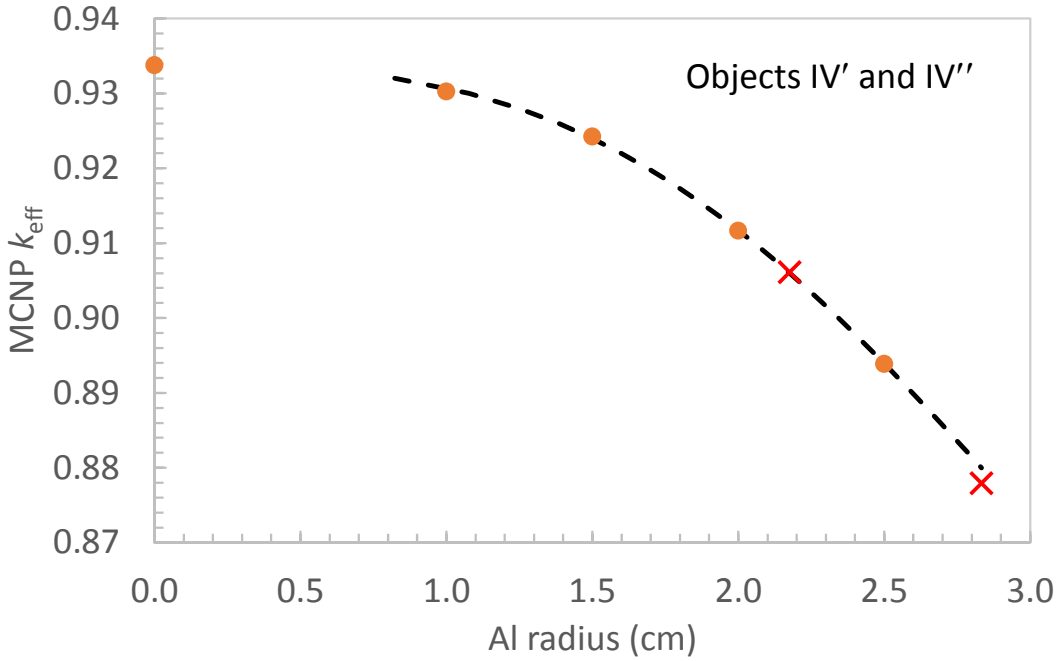

Fig. 4. k_{eff} vs the radius of a central Al ball.

Please notice that the inferred k_{eff} distributions can be influenced by the priors used. For example, in the case of objects IV′ and IV″, if one uses the information that the smallest possible Al ball has a radius of 2 cm, then k_{eff} values larger than 0.912 would not be inferred. This is a little problematic given that both objects IV′ and IV″ have detailed models that give k_{eff} values > 0.912. This highlights differences between the simple model used here, and the more detailed model used by Goorley to give the values listed in Table II. Please remember, Goorley used detailed measured properties of every shell and hemi-shell used to make these objects. We have here introduced a simplified four shell Al, HEU, Al, HDP plus outer can model that uses generic effective average densities. The radius of the central Al ball can be used as the model parameter that can be adjusted to match measured gamma-ray die-away curves, and thus obtain a k_{eff} inference. Perhaps we should drop the density of the HEU in the simple model to match Goorley's detailed calculations of objects IV′ and IV″. However, as discussed later, the calculated die-away curves are insensitive to the object changes considered here, if the k_{eff} is kept fixed, and thus additional complexity is not warranted if we only desire a k_{eff} inference. If we wished to make an absolute inference of the Al ball radius then greater care in model (prior) development would be required.

Model for objects IIIa and IIIb

These new models are based on the priors shown in Fig. 1 and have not yet been used to infer k_{eff} values for objects IIIa and IIIb from the corresponding experimental gamma-ray flux die-away curves. Instead, as discussed previously, the object IV model with HEU density modifications (see Fig. 2) has been used [4]. MCNP calculated k_{eff} values for the new models are given as functions of the Al inner radius in Fig. 5 (with all material densities held fixed). Tables V and VI list the corresponding relationships between the Al shell (or hemi-shell) inner radius and k_{eff}. Given the added complexity of these relationships compared to the previous figures, two quadratic fits were used for these objects, either side of r_i=3 cm.

Table V. The relationship between the inner radius of the object IIIa Al shell and k_{eff}.

k_{eff}	0.892	0.894	0.896	0.898	0.900	0.902	0.904	0.906	0.908	0.910
r_i (cm)	4.786	4.4125	4.1331	3.8998	3.6954	3.5112	3.3422	3.1851	3.0377	2.8886
k_{eff}	0.912	0.914	0.916	0.918	0.920	0.922	0.924	0.926	0.928	0.930
r_i (cm)	2.7339	2.5731	2.4052	2.2294	2.0442	1.8482	1.6391	1.4137	1.1678	0.8944
k_{eff}	0.932									
r_i (cm)	0.5812									

Table VI. The relationship between the inner radius of the object IIIb Al hemi-spherical shell and k_{eff}.

k_{eff}	0.914	0.916	0.918	0.920	0.922	0.924	0.926	0.928	0.930	0.932
r_i (cm)	4.6677	4.0454	3.6119	3.2583	2.9476	2.6234	2.2697	1.8767	1.4274	0.8871

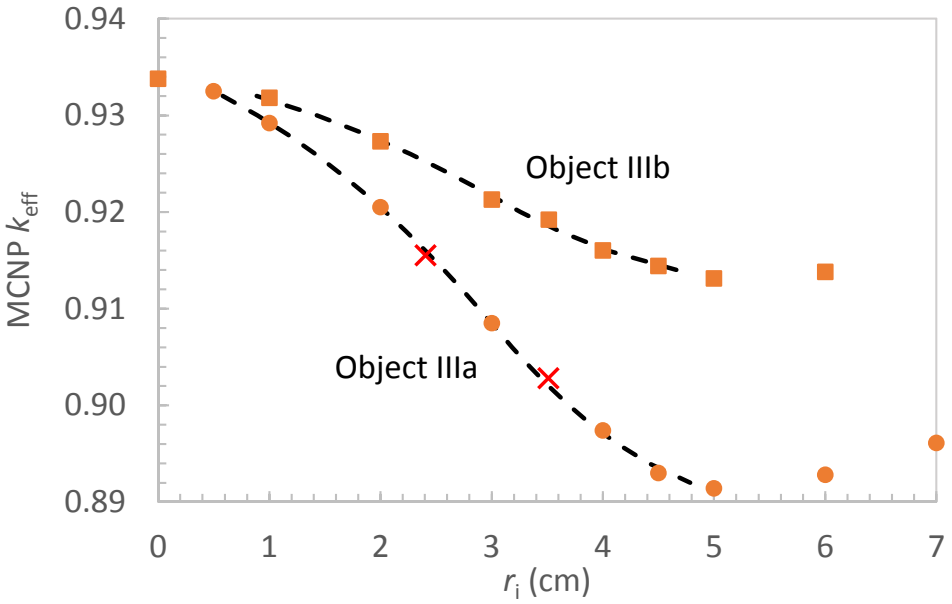

Fig. 5. MCNP calculated k_{eff} vs the inner radius of the object IIIa Al shell, and the inner radius of the object IIIb Al hemi-spherical shell (symbols).

As discussed in the previous section, please notice that the inferred k_{eff} distributions can be influenced by the prior(s) used. For example, in the case of object IIIa the Al shell prior restricts the inference of k_{eff} values to above 0.890. This is because of the minimum in k_{eff} as a function of the inner shell radius at r_i~5 cm (see Fig. 5), and can cause a bias to higher mean k_{eff} values for object IIIa inferences depending of the k_{eff} uncertainty. Likewise for object IIIb but the restriction is k_{eff}>0.912. This is problematic given that object IIIb has a "true" Al hemi-shell inner radius close to the corresponding turning point (see Fig. 5). To solve this problem we recommend using either the object IIIa model or one of the IV series models to access k_{eff} values below 0.914 when analyzing data from object IIIb. As discussed below, the different models are essentially degenerate in k_{eff} space, and thus the k_{eff} inferences should be essentially the same, independent of the model used (excluding the more subtle prior influencing effects mentioned above).

Calculations of the time dependent die-away of object IIIa are displayed is Fig. 6 for two different k_{eff} values. Here the DPF is assumed to be a delta spike. The orange circles show the "raw" calculation with a MCNP nps of 10^6, with r_i=3.5112 cm and corresponding k_{eff}=0.902 (see Table V). The Monte Carlo noise can be reduced by increasing the number of source particles (nps). The orange curve (that is difficult to see under the orange circles) is a three exponential fit to the k_{eff}=0.902 simulation. The black curve shows a three exponential fit to the corresponding k_{eff}=0.895 calculation. These calculations show the sensitivity of the observable (exiting gamma-ray flux) to changes in the k_{eff} of object IIIa like objects, and demonstrate the possibility of a k_{eff} inference (at least in principle). Of course, the true experimental situation is made more complex due to the non-delta-spike DPF source and die-away detector response. These considerations are beyond the scope of this study but reported elsewhere [4].

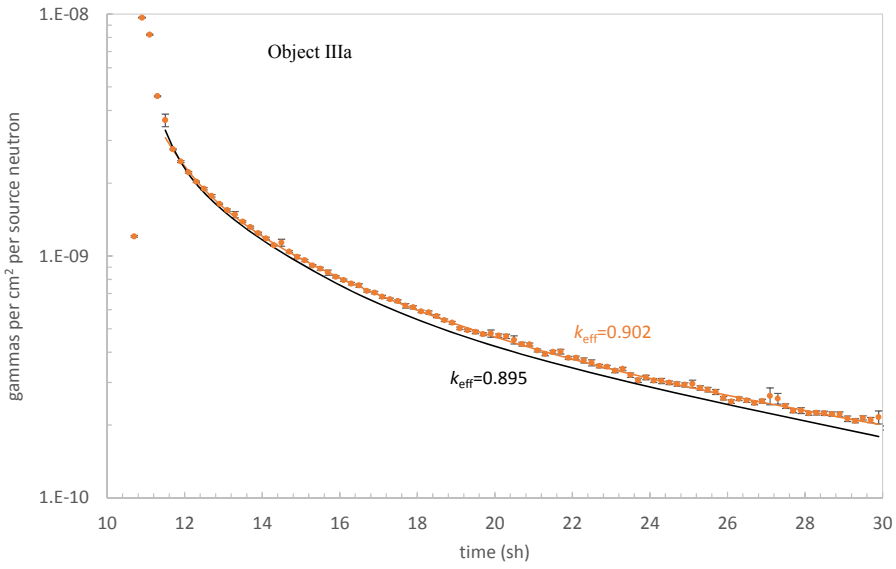

Fig. 6. Object IIIa MCNP calculations of the gamma-ray flux at the die-away detector 20 m from the object (see text for details).

Difference between objects with a fixed k_{eff}

The reason for the presented shell model is to address concerns expressed by others, about the simplicity of the previously used inference method where the density of the HEU in object IV was adjusted to infer the k_{eff} values of objects IV′, IV″, IIIa, and IIIb. Gamma-ray flux die-away calculations for four different objects with the same k_{eff}=0.912 are displayed in Fig. 7. The die-away curves for these four different objects (with the same k_{eff}) are almost identical, with differences much smaller than the differences associated with a 1.7% shift to k_{eff}=0.895 as demonstrated by the black curve in Fig. 7. This negates the necessity of applying our shell models to the existing series IV and III data, and demonstrates that a measurement of the die-away curve is effectively a measurement of the k_{eff} of the series IV and III objects, and not sensitive to the details of their SNM radial density distributions (at fixed k_{eff}).

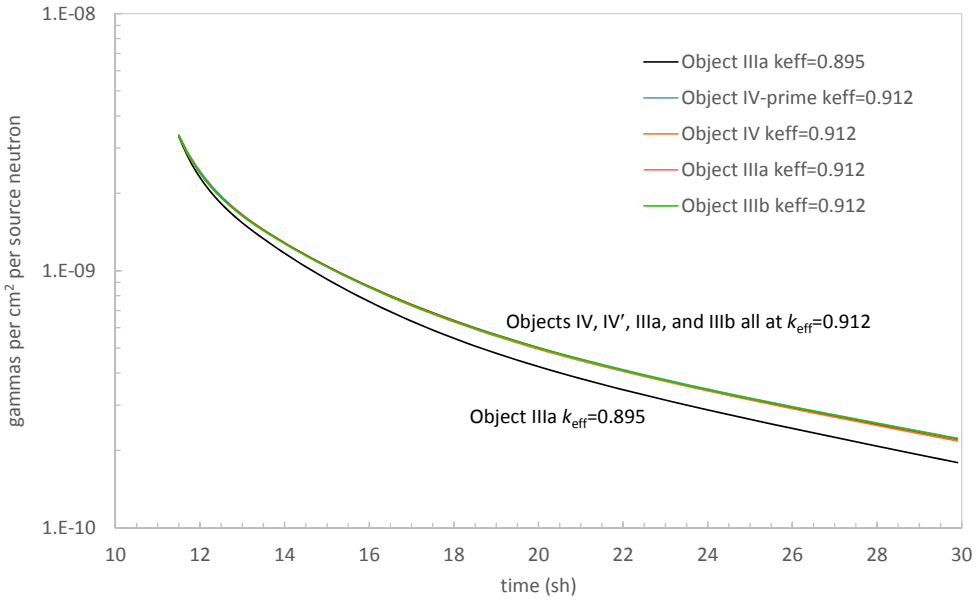

Fig. 7. Fits to MCNP calculated die-away gamma-ray flux curves for five objects. Notice that the four different objects with the same k_{eff} value of 0.912 have very similar die-away curves. This demonstrates that for similar objects with the same outer SNM and tamper configurations but differing SNM density distributions in the interior, the die-away curve is effectively a measure of the object's k_{eff} value.

Summary

We have introduced simple four and five layered models of objects IV′, IV″, IIIa, and IIIb, where a single Al radius can be changed, while keeping all material densities fixed. These models could be used as priors to match forward simulations to experimental die-away curves, and thus the inference of k_{eff} values from measurements. Fig. 7 demonstrates the insensitivity of the calculated die-away curves (with a delta-spike source and detector response) to different SNM radial distributions and symmetries, at a fixed k_{eff} value. These results show that we expect little difference in the inferences of object IIIa and IIIb k_{eff} values in switching between the different models (priors) discussed in this paper.

The results displayed in figures 6 and 7 show the sensitivity of the calculated die-away curves to changes in k_{eff} values. As previously discussed, the sensitivity to k_{eff} increases with increasing k_{eff} and will improve significantly with the change to plutonium test objects [5].

References

[1] E. Hutterer, The bomb without the boom, Los Alamos Science and Technology Magazine Issue October 2017.

[2] DeYoung et al, data corrected at the NDSE proof-of-principle facility at area-11 Nevada, private communications to M. T. Andrews.

[3] T. J. Goorley, A. DeYoung, M. Mitchell, and J. Hutchinson, Special Nuclear Material (SNM) Object II for Initial Neutron Diagnosed Subcritical Experiment (NDSE) Static Tests at NNSS Area 11, memorandum to M. Furlanetto, Jan 27, 2017. Object IV is Object II placed in a protective can to minimize the chance of a criticality accident. Plus additional private communications from J. T. Goorley to J. P. Lestone.

[4] M. T. Andrews and J. P. Lestone, Inferring the k_{eff} of NDSE Objects III and IV via Simple HEU Density Scaling, Los Alamos National Laboratory Report, LA-UR-19-2095 (January 2019).

[5] J. P. Lestone and M. T. Andrews, (U) NDSE Uncertainty Analysis, Los Alamos Controlled Publication, LA-CP-18-00373 (April 2018).